Journal of Intelligent Manufacturing (2020) 31:1243–1255
https://doi.org/10.1007/s10845-019-01509-5

Timely chatter identification for robotic drilling using a local maximum synchrosqueezing-based method

Jianfeng Tao[1] · Chengjin Qin[1] · Dengyu Xiao[1] · Haotian Shi[1] · Xiao Ling[1] · Bingchu Li[2] · Chengliang Liu[1]

Received: 16 March 2019 / Accepted: 25 October 2019 / Published online: 1 November 2019

Abstract

Induced by flexibility of the industrial robot, cutting tool or the workpiece, chatter in robotic machining process has detrimental effects on the surface quality, tool life and machining productivity. Consequently, accurate detection and timely suppression for such undesirable vibration is desperately needed to achieve high performance robotic machining. This paper presents a novel approach combining the notch filter and local maximum synchrosqueezing transform for the timely chatter identification in robotic drilling. The proposed approach is accomplished through the following steps. In the first step, the optimal matrix notch filter is designed to eliminate the interference of the spindle frequency and corresponding harmonic components to the measured acceleration signal. Subsequently, the high-resolution time–frequency information of the non-stationary filtered acceleration signal is acquired by employing local maximum synchrosqueezing transform (LMSST). On this basis, the filtered acceleration signal is divided into a finite number of equal-width frequency bands, and the corresponding sub-signal for each frequency band is obtained by summing the corresponding coefficient of the LMSST. Finally, to accurately depict the non-uniformity of energy distribution during the chatter incubation process, the statistical energy entropy is calculated and utilized as the indicator to detect chatter online. The effectiveness of the proposed approach is validated by a large number of robot drilling experiments with different cutting tools, workpiece materials and machining parameters. The results show that the presented local maximum synchrosqueezing-based approach can effectively recognize the chatter at an early stage during its incubation and development process.

Keywords Robotic drilling · Chatter identification · Optimal matrix notch filter · Local maximum synchrosqueezing-based method · Time–frequency information · Energy entropy

✉ Chengjin Qin
qinchengjin@sjtu.edu.cn

Jianfeng Tao
jftao@sjtu.edu.cn

Dengyu Xiao
xiaodengyu@sjtu.edu.cn

Haotian Shi
sht_015020910058@sjtu.edu.cn

Xiao Ling
lingxiao@sjtu.edu.cn

Bingchu Li
bclicsu@sina.com

Chengliang Liu
chlliu@sjtu.edu.cn

[1] State Key Laboratory of Mechanical System and Vibration, School of Mechanical Engineering, Shanghai Jiao Tong University, Shanghai 200240, China

[2] School of Mechanical Engineering, University of Shanghai for Science and Technology, Shanghai 200093, China

Introduction

Industrial robots equipped with customized drilling and riveting end effectors can significantly improve the quality and efficiency of aviation manufacturing and assembly (Zeng et al. 2017; Bi and Liang 2011; Frommknecht et al. 2017; Mei et al. 2015). However, compared with the traditional machine tools, high-performance robotic drilling is still a challenging task due to the various types of errors affecting pose accuracy as well as the relatively low stiffness of robotic joints and the end effector (Iglesias et al. 2015; Chen and Dong 2013; Lin et al. 2017). Robotic drilling system is more prone to chatter during the machining process, which will result in poor surface finish, shortened tool life and decreased machining productivity (Yuan et al. 2018; Munoa et al. 2016; Bu et al. 2017). To reduce and eliminate the negative effects on the machining system, many efforts have been devoted to the modelling, predicting, detecting and controlling such undesirable instability (Mousavi et al. 2017; Wang et al. 2017; Lu et al. 2015; Pour and Torabizadeh 2016; Cordes et al. 2019; Qin et al. 2017a, b, 2018; Tong et al. 2019; Somkiat 2011; Yuan et al. 2019).

For the sake of chatter avoidance, researchers have proposed many stability analysis methods to construct the stability lobe diagrams, including numerical methods, analytical methods, and semi-analytical methods (Li and Liu 2008; Insperger and Stepan 2004; Altintas et al. 2008; Qin et al. 2019). However, the accuracy of stability lobe diagrams mainly depends on the dynamics model of machining process, for which errors are always inevitable. Chatter may still occur with the selected stable cutting parameters according to the stability analysis. Meanwhile, it is quite complicated for workshop workers to fully understand and grasp the cutting dynamics. Alternatively, it is practical and essential to detect and recognize chatter as early as possible during the transition stage, so as to adopt appropriate suppression method.

To accurately identify the chatter, it is of vital importance to select the most appropriate and sensitive signals, employ effective processing methods, and extract sensitive chatter indicators. It has been well recognized that vibration signals can most fully reflect the chatter transition process, and have the advantages of low cost and easy measurement (Kuljanic et al. 2009; Tao et al. 2019b). For these reasons, vibration signals are applicable under industrial conditions, and thus commonly used in machining chatter monitoring (Tao et al. 2019a; Ye et al. 2018; Lamraoui et al. 2014a; Fu et al. 2016, 2019; Sun and Xiong 2016; Ji et al. 2017). Besides, scholars have also utilized other sensor signals to monitor and detect chatter, including cutting force signals (Wang et al. 2018; Huang et al. 2013; Tangjitsitcharoen et al. 2015; Liu et al. 2017), motor current signals (Liu et al. 2011, 2016; Aslan and Altintas 2018), angular speed signals (Lamraoui et al. 2014b), and sound signals (Thaler et al. 2014; Cao et al. 2017). Due to the regenerative mechanism, the occurrence of chatter is commonly accompanied by changes in frequency components and energy distribution (Tao et al. 2019a; Ye et al. 2018; Lamraoui et al. 2014a, b; Fu et al. 2016, 2019; Sun and Xiong 2016; Ji et al. 2017; Wang et al. 2018; Huang et al. 2013; Tangjitsitcharoen et al. 2015; Liu et al. 2011, 2016, 2017; Aslan and Altintas 2018; Thaler et al. 2014; Cao et al. 2017). To keenly capture the chatter characteristics, many time–frequency analysis methods have been utilized for cutting status monitoring, including short-time Fourier transform (STFT) (Thaler et al. 2014), wavelet transform (WT) (Sun and Xiong 2016; Tangjitsitcharoen et al. 2015; Liu et al. 2017), empirical mode decomposition (EMD) (Fu et al. 2016; Ji et al. 2017; Liu et al. 2017; Ji et al. 2018) and variational mode decomposition (VMD) (Zhang et al. 2016; Liu et al. 2018; Yang et al. 2019). However, restricted by the Heisenberg uncertainty principle, the classical processing methods suffer from relatively low time–frequency resolution (Yu et al. 2017). In addition, a review of the literature shows that the measured signals during machining processes are usually nonlinear and non-stationary. Therefore, they cannot be competent to characterize the nonstationary behavior of the measured signals accurately.

Recently, some researchers have tried to employ more powerful time–frequency processing methods with higher energy concentration to detect chatter. For instance, Cao et al. (Lamraoui et al. 2014b) presented a chatter detection method for high-speed milling process, in which time–frequency representation of the sound signals was obtained by the synchrosqueezing transform (SST). However, in the synchrosqueezing processing of time–frequency coefficients, the unexpected noise has to be gathered into the SST result. Also, Tao et al. (2019a) proposed a synchroextracting-based method for the early chatter detection of robotic drilling operations. Due to lack of perfect signal reconstruction, the synchroextracting transform (SET) may suffer large reconstruction errors when processing strong non-stationary signals. On the other hand, it has been found that during the early stage of chatter, although the spindle frequency component and its corresponding harmonics still plays a major role, chatter components have appeared and are distributed in a wide frequency band (Liu et al. 2016; Wan et al. 2018). Therefore, it is necessary to eliminate the disturbance of spindle frequency and corresponding harmonic components to the measured acceleration signal. To realize accurate and timely chatter identification, this paper develops a novel identification method combining the notch filter and local maximum synchrosqueezing transform for robotic drilling process, in which weak chatter features during early stage of inoculation can be keenly captured. The rest of this paper is organized as follows. In second section, the optimal matrix notch filter is designed to eliminate the interference of the spindle frequency and corresponding harmonic components to the measured signal. Then, the LMSST is employed to obtain high-resolution time–frequency information of the non-stationary filtered acceleration signal. On this basis, the proposed identification algorithm is proposed in detail. In third section, the experimental setup is presented, and the effectiveness of the proposed approach is validated by a large number of robot drilling experiments with different drilling parameters and workpiece materials. The conclusion is drawn in the last section.

Local maximum synchrosqueezing-based method

Optimal matrix notch filter

As mentioned above, it is of vital importance to accurately remove the spindle frequency and corresponding harmonic components from the measured signals for chatter monitoring. Compared with finite impulse response (FIR) filter, the order of infinite impulse response (IIR) filter is much lower under the same frequency requirement. Notch filter belongs to the IIR filter, and is an effective means of eliminating narrowband or sinusoidal interference (Tseng and Pei 2001). Denote ω_N as be the notch frequency, then the transfer function $H(z)$ of the traditional notch filter is defined as:

$$H(z) = \frac{1 - 2\cos(\omega_N)z^{-1} + z^{-2}}{1 - 2\eta\cos(\omega_N)z^{-1} + \eta^2 z^{-2}} \tag{1}$$

where η denotes the pole radius. The notch bandwidth B_w is defined by $B_w = \pi(1-\eta)$. When the pole radius η approaches 1, the notch filter is close to the ideal one.

However, the traditional notch filter suffers a long transition stage, making it difficult to obtain good filtering performance when processing short data. Consequently, researchers were trying to suppress the transition stage to optimize the conventional notch filter (Piskorowski 2010, 2012). The key to designing the notch filter is obtaining the transfer function with frequency response as close as possible to the ideal notch filter (Vaccaro and Harrison 1996; Han and Zhang 2010). Define the signal of length N to be filtered as $\mathbf{s}_i = [\mathbf{s}_i(1), \mathbf{s}_i(2), \ldots, \mathbf{s}_i(N)]$, the output signal of the notch filter as $\mathbf{s}_o = [\mathbf{s}_o(1), \mathbf{s}_o(2), \ldots, \mathbf{s}_o(N)]$, then the designed optimal notch matrix F_N obtained via certain optimal criterion should satisfy:

$$\mathbf{S}_o = \mathbf{F}_{\omega_N}\mathbf{S}_i \tag{2}$$

In order to solve the notch matrix F_N, we define a complex column vector as $\mathbf{q}(\omega) = [1, e^{j\omega}, e^{j2\omega}, \ldots, e^{j(N-1)\omega}]^T$. Obviously, the designed optimal notch matrix should approximate the frequency response as close as possible to the ideal notch filter, that is

$$\mathbf{F}_{\omega_N}\mathbf{q}(\omega) = \begin{cases} \mathbf{0}, & \omega = \omega_N \\ \mathbf{q}(\omega), & \omega \neq \omega_N \end{cases} \tag{3}$$

Introduce a small enough positive number ξ, the band-pass of the designed notch filter will be $B_p = [0, \omega_N - \xi] \cup [0, \omega_N + \xi]$. The first step to solve the notch matrix F_N is discretizing the band-pass B_p into M frequency points of equal distance, i.e.,

$$\omega_k = k(\pi - 2\xi)/M, \quad k = 1, 2, \ldots, M \tag{4}$$

Substituting the above discrete frequency points and the notch frequency ω_N into the complex column vector $\mathbf{q}(\omega)$, the following matrices can be obtained:

$$\begin{cases} \mathbf{Q}_R = [\mathbf{q}_R(\omega_1), \mathbf{q}_R(\omega_2), \ldots, \mathbf{q}_R(\omega_M)] \\ \mathbf{Q}_I = [\mathbf{q}_I(\omega_1), \mathbf{q}_I(\omega_2), \ldots, \mathbf{q}_I(\omega_M)] \\ \mathbf{Q} = [\mathbf{Q}_R, \mathbf{Q}_I] \\ \mathbf{P} = [\mathbf{q}_R(\omega_N), \mathbf{q}_I(\omega_N)] \end{cases} \tag{5}$$

where the subscripts R and I denote real and imaginary parts of the complex number, respectively. According to the frequency response of ideal notch filter, i.e., Eq. (3), the matrices $\boldsymbol{Q}$ with size $N \times 2M$, $\boldsymbol{P}$ and F_N should satisfy the following relationship:

$$\begin{cases} \mathbf{Q} = \mathbf{F}_{\omega_N}\mathbf{Q} \\ \mathbf{0} = \mathbf{F}_{\omega_N}\mathbf{P} \end{cases} \tag{6}$$

Define $\mathbf{q}_i$ and $\mathbf{f}_i$ as the i-th column vector of $\mathbf{Q}^T$ and $(F_{\omega_N})^T$, $i = 1, 2, \ldots, N$. Then, by utilizing the least squares method, the following optimization model can be established:

$$\begin{aligned} &\min J_i = \left\| \mathbf{Q}^T\mathbf{f}_i - \mathbf{q}_i \right\|_2^2 \\ &\text{s.t.} \quad \mathbf{P}^T\mathbf{f}_i = \mathbf{0} \end{aligned} \tag{7}$$

To simplify the derivation, define a new matrix as $\mathbf{G} = \mathbf{Q}\mathbf{Q}^T$. Solving Eq. (7) by employing Lagrangian multiplier method, the column vector $\mathbf{f}_i$ can be obtained:

$$\mathbf{f}_i = \mathbf{G}^{-1}\mathbf{Q}_i\mathbf{q}_i - \mathbf{G}^{-1}\mathbf{P}^T(\mathbf{P}\mathbf{G}^{-1}\mathbf{P}^T)^{-1}\mathbf{P}\mathbf{G}^{-1}\mathbf{Q}_i\mathbf{q}_i \tag{8}$$

On this basis, the designed optimal notch matrix F_N can be finally obtained as:

$$\mathbf{F}_{\omega_N} = \mathbf{I} - \mathbf{P}(\mathbf{P}^T\mathbf{G}\mathbf{P})\mathbf{P}^T\mathbf{G}^T \tag{9}$$

Local maximum synchrosqueezing transform

The synchroextracting transform (SET) has been proved to be a highly concentrated time–frequency analysis method (Yu et al. 2017). However, due to lack of perfect signal reconstruction, it may suffer large reconstruction errors when processing strong non-stationary signals. Recently, Yu et al. (2019) developed the local maximum synchrosqueezing transform (LMSST), which can be utilized to effectively extract high-precision time–frequency information from signals with heavy noise and perfectly reconstruct the signals.

LMSST belongs to a post-processing technique of the STFT. The STFT of the signal $s(u)$ with respect to the real and even window $g(u)$ is defined as:

$$STFT_s(t,\omega) = \int_{-\infty}^{\infty} s(u)g(u-t)e^{-j\omega(u-t)}du \tag{10}$$

where g denotes the time-domain compactly supported window, and is often chosen as a real couple function whose energy is concentrated at low frequencies. As time t changes continuously, the window g moves on the time axis. As a consequence, the signal $s(u)$ is gradually analyzed.

Define $s(u)$ as a multi-component signal with a certain frequency separation, namely

$$s(u) = \sum_{k=1}^{n} s_k(u) = \sum_{k=1}^{n} A_k(u)e^{j\phi_k(u)} \tag{11}$$

where $A_k(u)$ and $\phi_k(u)$ represent the instantaneous amplitude and the instantaneous angular position of $s_k(u)$, respectively.

Mathematically, the STFT is to calculate the Fourier transform of $s(u)g(u-t)$ in a short time. Based on the assumption that $A_k'(t)$ and $\phi_k''(t)$ are small enough (Yu et al. 2019), we can expand $A_k(u)$ and $\phi_k(u)$ at time t using the Taylor expansion, which is written as $A_k(u) = A_k(t)$ and $\phi_k(u) = \phi_k(t) + \phi_k'(t)(u-t)$. Consequently, the signal $s(u)$ can be rewritten as $s(u) = \sum_{k=1}^{n} A_k(t)e^{j\phi_k(t)+j\phi_k'(t)(u-t)}$. Substitute it into STFT, i.e., Eq. (10), one can obtain:

$$STFT_s(t,\omega) = \sum_{k=1}^{n} A_k(t)e^{j\phi_k(t)}\hat{g}(\omega - \phi_k'(t)) \tag{12}$$

where $\hat{g}$ denotes the Fourier transform of window function g.

In-depth analysis of Eq. (12) reveals that the spectrogram concentrates on the time–frequency trajectories with a smeared energy distribution, i.e.,

$$\left|STFT_s(t,\omega)\right| = \sum_{k=1}^{n} A_k(t)\hat{g}(\omega - \phi_k'(t)) \tag{13}$$

By searching for the local maximum of the spectrogram in the frequency direction, a novel frequency-reassignment operator based on Eq. (13) is defined as

$$\zeta_m(t,\omega)\begin{cases} \arg\max_{\omega} \left|STFT_s(t,\omega)\right|, & \omega \in [\omega-\Delta, \omega+\Delta], \quad if\left|STFT_s(t,\omega)\right| \neq 0 \\ 0, & if\left|STFT_s(t,\omega)\right| = 0 \end{cases} \tag{14}$$

where Δ denotes the frequency support of the window function g.

Since the Fourier transform of the window function reaches the maximum at zero, Eq. (14) can be further simplified as

$$\zeta_m(t,\omega)\begin{cases} \phi_k'(t), & if\,\omega \in [\omega-\Delta, \omega+\Delta] \\ 0, & \text{otherwise} \end{cases} \tag{15}$$

To obtain the ideal time–frequency analysis representation and retain the perfect reconstruction ability, all of the smeared time–frequency coefficients should be reassigned into the time–frequency trajectories along the frequency direction. Consequently, the local maximum synchrosqueezing transform that can generate a more highly concentrated time–frequency representation can be expressed as

$$LMSST_s(t,\eta) = \int_{-\infty}^{\infty} STFT_s(t,\omega)\delta(\eta - \zeta_m(t,\omega))d\omega \tag{16}$$

where δ represents the Dirac function.

Equation (16) ensures that the time–frequency representation generated by LMSST can be well approximated to ideal time–frequency analysis representation. By integrating function $LMSST_s(t,\eta)$, one can get the following expression

$$\begin{aligned} \int_{-\infty}^{+\infty} LMSST_s(t,\eta)d\eta &= \int_{-\infty}^{+\infty}\int_{-\infty}^{+\infty} STFT_s(t,\omega)\delta(\eta \\ &\quad - \zeta_m(t,\omega))d\omega d\eta \\ &= \int_{-\infty}^{+\infty} STFT_s(t,\omega)\int_{-\infty}^{+\infty}\delta(\eta \\ &\quad - \zeta_m(t,\omega))d\eta d\omega \\ &= \int_{-\infty}^{+\infty} STFT_s(t,\omega)d\omega \\ &= 2\pi\int_{-\infty}^{+\infty} s(u)g(u-t)\delta(u-t)du \\ &= (2\pi g(0))s(t) \end{aligned} \tag{17}$$

Consequently, the original signal can be perfectly recovered by

$$s(t) = (2\pi g(0))^{-1}\int_{-\infty}^{+\infty} LMSST_s(t,\eta)d\eta \tag{18}$$

The proposed identification method

Chatter vibration in machining processes arises from a self-excitation mechanism between the tool and the workpiece. Due to the regenerative mechanism, the occurrence of chatter will cause changes in frequency components and energy distribution. With the development of chatter, new dominant frequency component will appear near the natural frequency of the system, and the energy is gradually absorbed by the chatter frequency. During the early stage of chatter, the chatter characteristic is extremely weak. Although the spindle frequency component and its corresponding harmonics still plays a major role, chatter components have appeared and distributed in a wide frequency band at this stage. Therefore, to achieve accurate and timely chatter identification, it is of vital importance to fully remove the spindle frequency and corresponding harmonic components from the vibration signal, obtain high-resolution time–frequency representation and keenly capture the change of energy distribution of the filtered vibration signal.

Inspired by the above analysis, we present a novel robotic drilling chatter identification algorithm based on the matrix notch filter and LMSST. The optimal matrix notch filter is designed to eliminate the disturbance of spindle frequency and corresponding harmonic components to the vibration signal. Then, the LMSST is employed to obtain high-resolution time–frequency information of the non-stationary filtered acceleration signal. On this basis, the filtered vibration signal is divided into finite equal-width frequency bands, and the corresponding sub-signal for each frequency band is obtained by summing the corresponding coefficient of the LMSST. Finally, the energy entropy is calculated and utilized as the indicator to accurately depict the non-uniformity of energy distribution during the chatter incubation process.

The detailed implementation steps of the proposed robotic drilling chatter identification method are specifically explained below. First, the signal length N is determined according to the signal sampling period T and the time interval τ of the chatter identification:

$$N = 2\tau/T \tag{19}$$

Let $\mathbf{u}_i$ be the measured acceleration signal, and ω_{s1}, ω_{s2}, …, ω_{sk} be the spindle frequency and corresponding harmonics. Subsequently, the corresponding notch matrices $\mathbf{F}_{\omega_{s1}}, \mathbf{F}_{\omega_{s2}}, \ldots, \mathbf{F}_{\omega_{sk}}$ are designed by the method presented in "Optimal matrix notch filter" section. By fully removing the spindle frequency and its corresponding harmonics, the filtered vibration signal $\mathbf{u}_o$ can be acquired as follows:

$$\mathbf{u}_o = \mathbf{F}\mathbf{u}_i = (\mathbf{F}_{\omega_{sk}} \cdots \mathbf{F}_{\omega_{s2}} \mathbf{F}_{\omega_{s1}})\mathbf{u}_i \tag{20}$$

Then, the accurate time–frequency information of the non-stationary filtered acceleration signal is obtained by employing the LMSST, namely

$$LMSST_u(t,\omega) = \int_{-\infty}^{\infty} STFT_u(t,\omega)\delta(\omega - \zeta_m(t,\omega))d\omega \tag{21}$$

To make full use of the time–frequency information of the filtered acceleration signal and keenly capture its energy distribution changes, it is divided into a finite number of equidistant frequency bands, i.e., $f_b = (1/T)/2/m$, where m denotes the number of bandwidth. Since all of the smeared time–frequency coefficients have been reassigned into their time–frequency regions, the corresponding sub-signal for each frequency band can be reconstructed by summing the corresponding coefficient of the LMSST, that is

$$u_h(t)=(2\pi g(0))^{-1} \int_{(h-1)f_b}^{hf_b} LMSST_u(t,\omega)d\omega, \quad h = 1, 2, \ldots, m \tag{22}$$

Finally, to accurately depict the non-uniformity of energy distribution during the chatter incubation process, the statistical energy entropy is calculated and utilized as the indicator to detect chatter online. The energy contained in each reconstructed sub-signal is defined as

$$E_h = \sum_{j=1}^{N} u_h(t_j)^2, \quad h = 1, 2, \ldots, m \tag{23}$$

On this basis, the statistical energy entropy LMSSTE can be calculated as

$$\text{LMSSTE} = \sum_{h=1}^{m} E_h \ln(E_h) \tag{24}$$

It is noted that the energy entropy of the measured acceleration signal is calculated online during the robotic drilling process by utilizing the proposed identification algorithm, and simultaneously compared with the selected chatter threshold. When the energy entropy exceeds the threshold, chatter is thought to occur in the robotic drilling process and the subsequent chatter suppression should be conducted as soon as possible. Moreover, the determination of chatter threshold is also extremely vital for chatter identification. Therefore, it is determined based on plenty of robotic drilling experiments with different cutting tools, workpiece materials and cutting parameters, ensuring the selected threshold is applicable for different robotic drilling condition.

Validation and analysis

Experimental setup

As illustrated in Fig. 1, the robotic drilling experiments were conducted to verify the proposed method on a self-designed robotic drilling system. It contains a KUKA KR 270 industrial, a sliding guide, a measurement control system, a self-designed drilling end effector, workpiece and corresponding holding fixture. The dedicated end effector mainly consists of a robot flange interface, a feed unit, a spindle unit, a normal detection unit, a visual measurement unit, and a pressure foot unit. The drilling motion is achieved by the feed unit and the spindle unit. The normal detection unit includes four laser displacement sensors uniformly arranged on the circumference, and is utilized for accurately obtaining the normal of the workpiece. The exact position of the reference hole is determined by the visual measurement unit. In order to increase the stiffness of the system as much as possible, the pressure foot is designed to provide a large pressing force during the robot drilling process. Figure 2 illustrates two

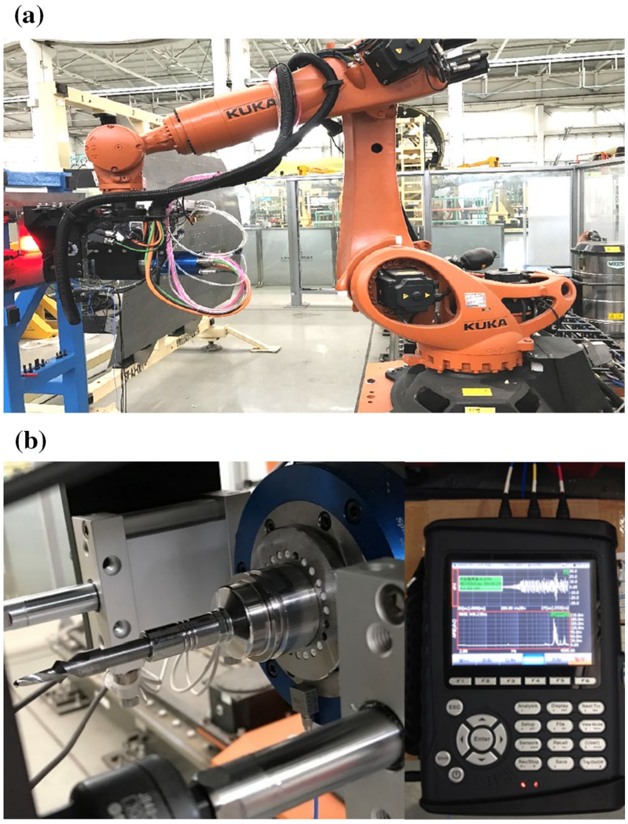

Fig. 1 The experimental setup: **a** the self-designed robotic drilling system and **b** the drilling tool with a PCB 356A24 accelerometer and the Crystal Instruments CoCo-80

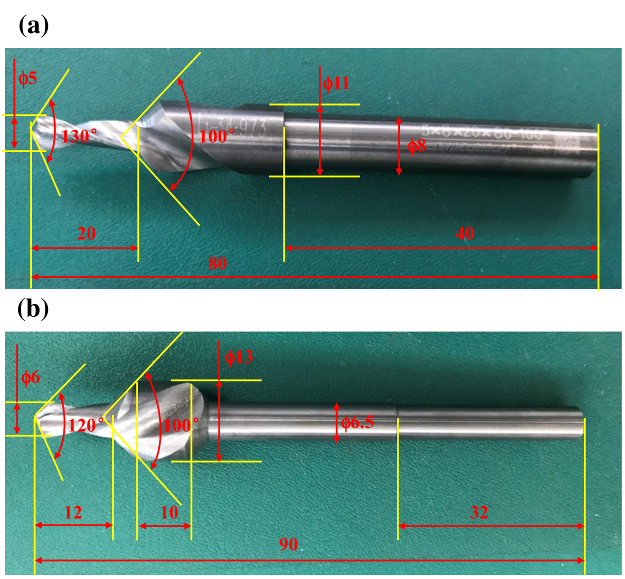

Fig. 2 Geometric parameters of the drilling-countersinking tools: **a** tool I with 5 mm and 130° point angle and **b** tool II with 6 mm diameter and 120° point angle

uncoated hard alloy steel drilling-countersinking tools with different geometric parameters that used in the robotic drilling tests. The tool I has 5 mm diameter and 130° point angle, and the tool II has 6 mm diameter, and 120° point angle. Meanwhile, both the countersink angle of tool I and tool II are 100°. In order to automatically identify robotic drilling chatter online, the vibration signals were measured and acquired by the PCB 356A24 accelerometer and the Crystal Instruments CoCo-80. Besides, the sampling frequency was set as 10,240 Hz.

Results and analysis

The effectiveness of the proposed identification method are validated by robotic drilling experiments with different drilling parameters and workpiece materials. It should be noted that to better observe the experimental process and evaluate the experimental results, the robotic drilling tests were conducted without lubrication and cooling. Actually, in the experiments, it is found that whether or not there is cooling and lubrication, the vibration signal has a similar trend when the chatter occurs. Therefore, the proposed method can be used for both with and without lubrication and cooling. The workpiece was aluminum alloy 7075 and 6061. During the robotic drilling tests, the spindle speed varied from 1800 to 4500 rpm and the feed rate from 0.9 to 9.6 mm/s. At the same time, the drilling depth was set as 6 mm and the pressing force was set as 0.12 MPa.

To realize timely and accurate detection of robotic drilling chatter, we present a novel identification method combining the matrix notch filter and local maximum synchrosqueezing transform. First, the matrix notch filter is designed to accurately remove the spindle frequency and its corresponding harmonic components from the measured vibration signals. Subsequently, the local maximum synchrosqueezing transform (LMSST) is employed to obtain high-resolution time–frequency information of the non-stationary filtered acceleration signal. Then, the filtered vibration signal is divided into finite equal-width frequency bands, and the corresponding sub-signal for each frequency band is obtained by summing the corresponding coefficient of the LMSST. Finally, to accurately depict the non-uniformity of energy distribution during the chatter incubation process, the statistical energy entropy is calculated and utilized as the indicator to detect robotic drilling chatter online. During the chatter identification, the measured vibration signal within 50 ms is processed every 25 ms. Since the sampling frequency was set as 10,240 Hz, the length of the sliding window is selected as 512 sample data with overlapping.

To begin with, we conducted robotic drilling tests with tool I and aluminum alloy 7075 under different drilling parameters. Figure 3 illustrates the time-domain diagram, the identification result and the time–frequency spectrogram

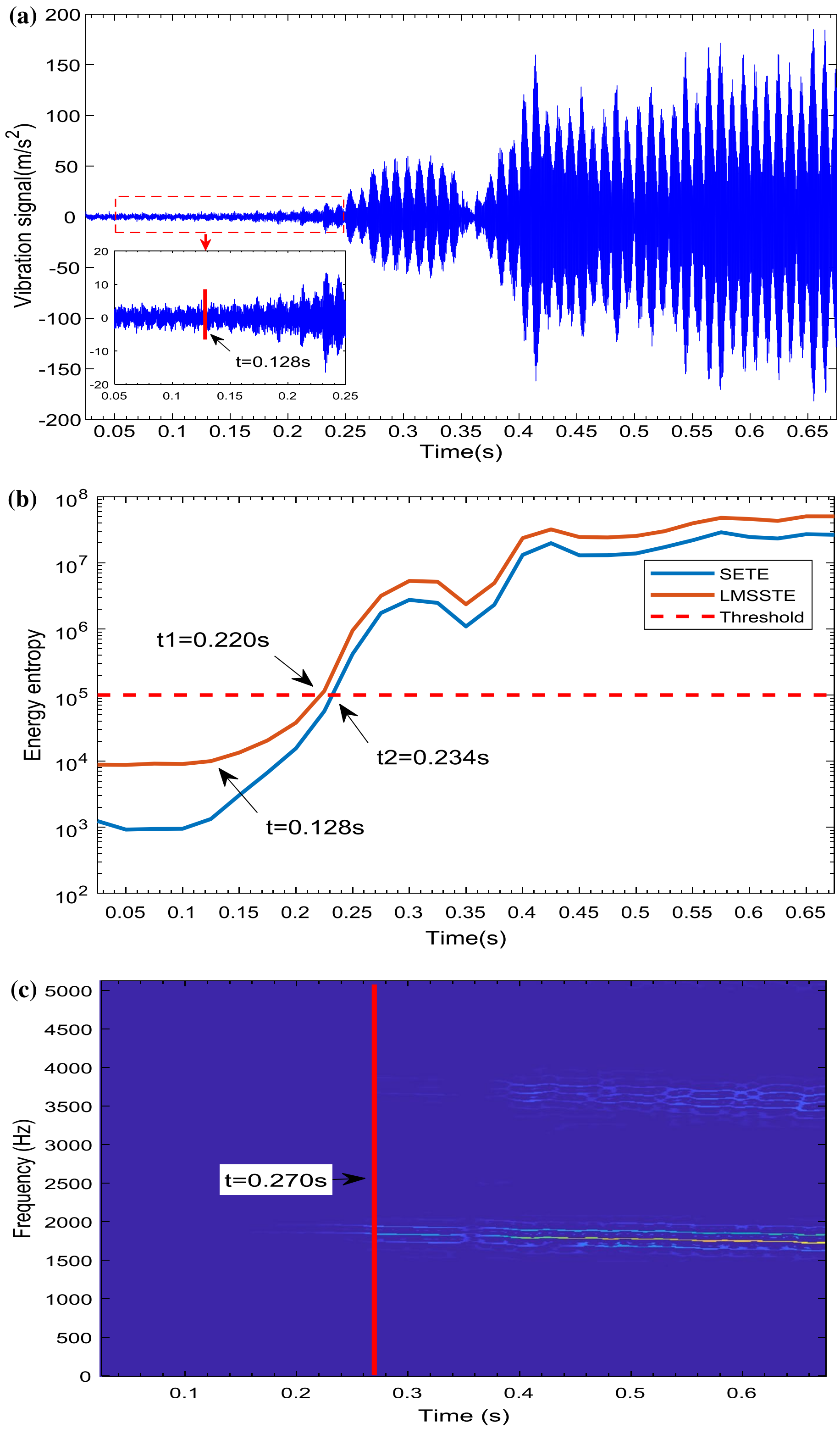

Fig. 3 The monitoring result and SET spectrogram for vibration signal with spindle speed 3000 rpm and feed rate 1.0 mm/s

for the vibration signal. The spindle speed was 3000 rpm, and feed rate was 1.0 mm/s. According to Fig. 3a, it is seen that the amplitude of the vibration signal increases rapidly after $t = 0.263$ s. Robotic drilling chatter occurs during the drilling process under this cutting parameters, and the amplitude of the vibration signal even reached 185 m/s^2 after the chatter was fully developed. At the beginning, energy entropy is relatively small and grows slowly. However, it can

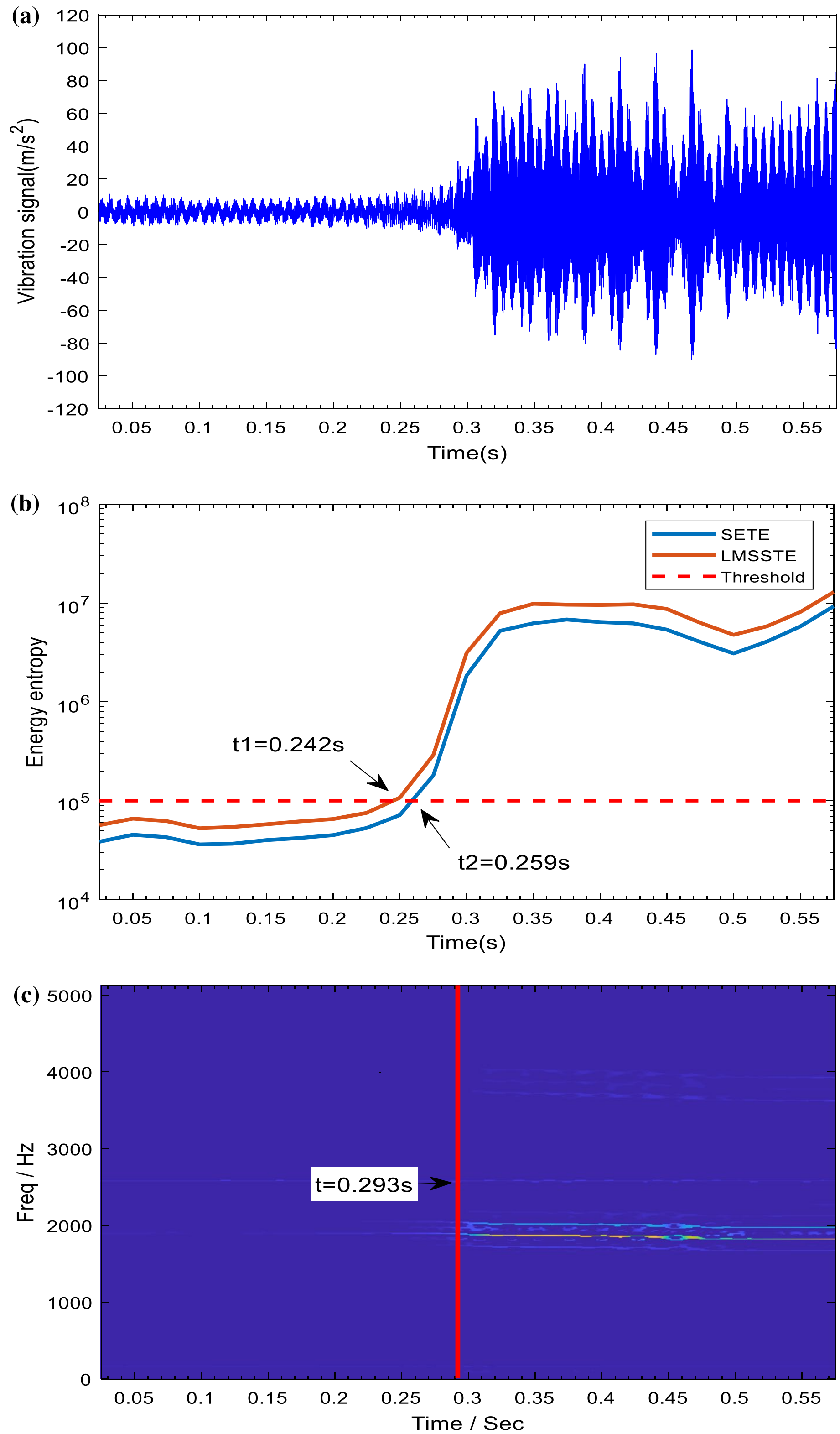

Fig. 4 The monitoring result and time–frequency spectrogram for the vibration signals with spindle speed 4500 rpm and feed rate 3.2 mm/s

be seen from Fig. 3b that the energy entropy of the vibration signal increases rapidly after $t=0.128$ s. Look closely at the corresponding time interval in Fig. 3a, it is found that the amplitude of the vibration signal begins to increase after $t=0.128$ s. Therefore, the selected statistical energy entropy is very sensitive to the change of energy distribution. According to Fig. 3b, the chatter is recognized at around $t1=0.220$ s by the proposed method. As shown in Fig. 3c,

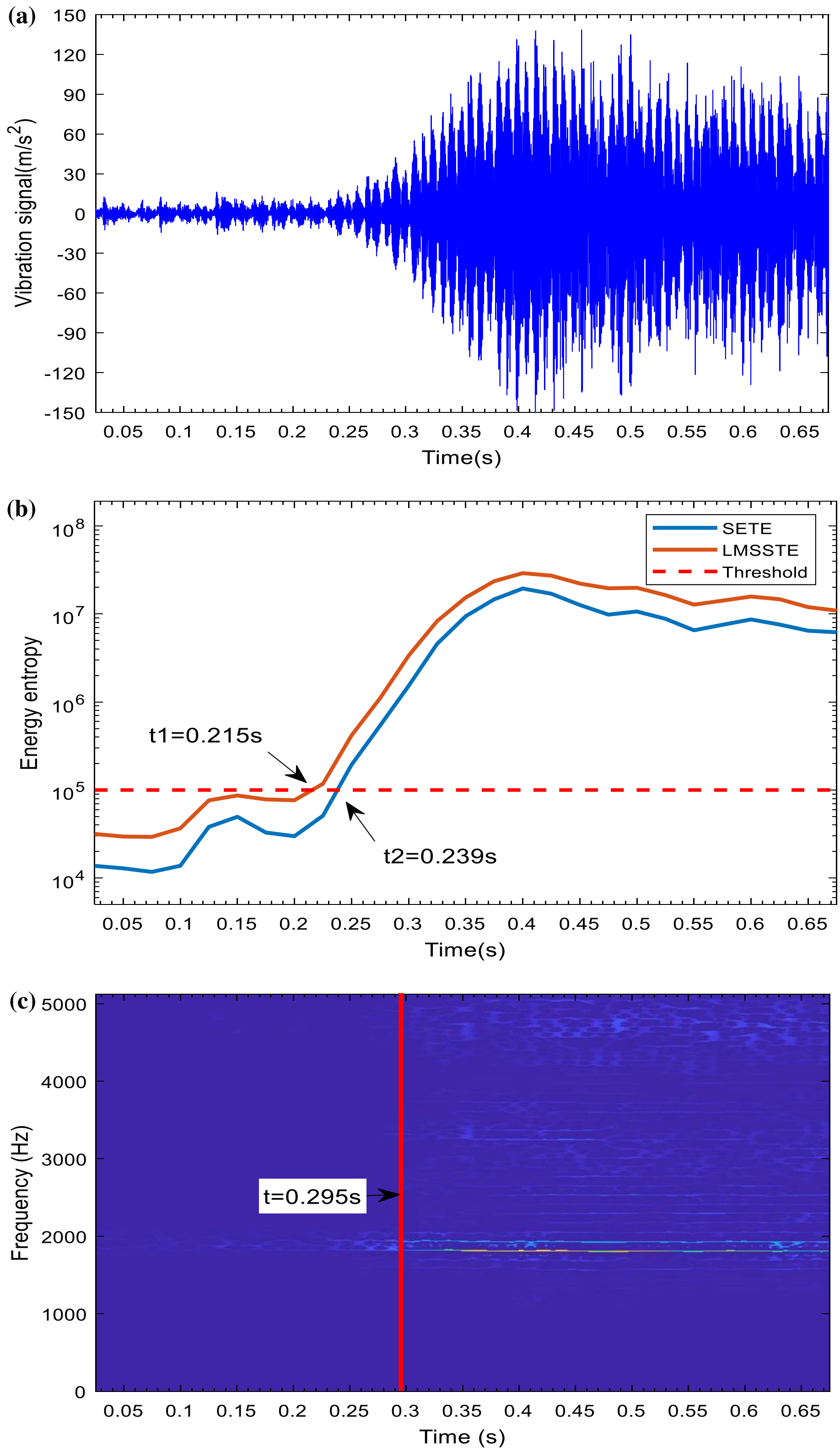

Fig. 5 The time-domain diagrams and SET spectrogram of vibration signals with spindle speed 3600 rpm and feed rate 3.6 mm/s

obvious chatter frequency appeared around $t = 0.270$ s in the high-resolution time–frequency spectrogram. Comparison between the time when chatter is detected and the time when obvious chatter frequency occurs shows that the proposed identification algorithm can effectively recognize the chatter before it is fully developed, which leaves valuable time for the subsequent chatter suppression measures. Moreover, Fig. 3b demonstrates that the proposed identification

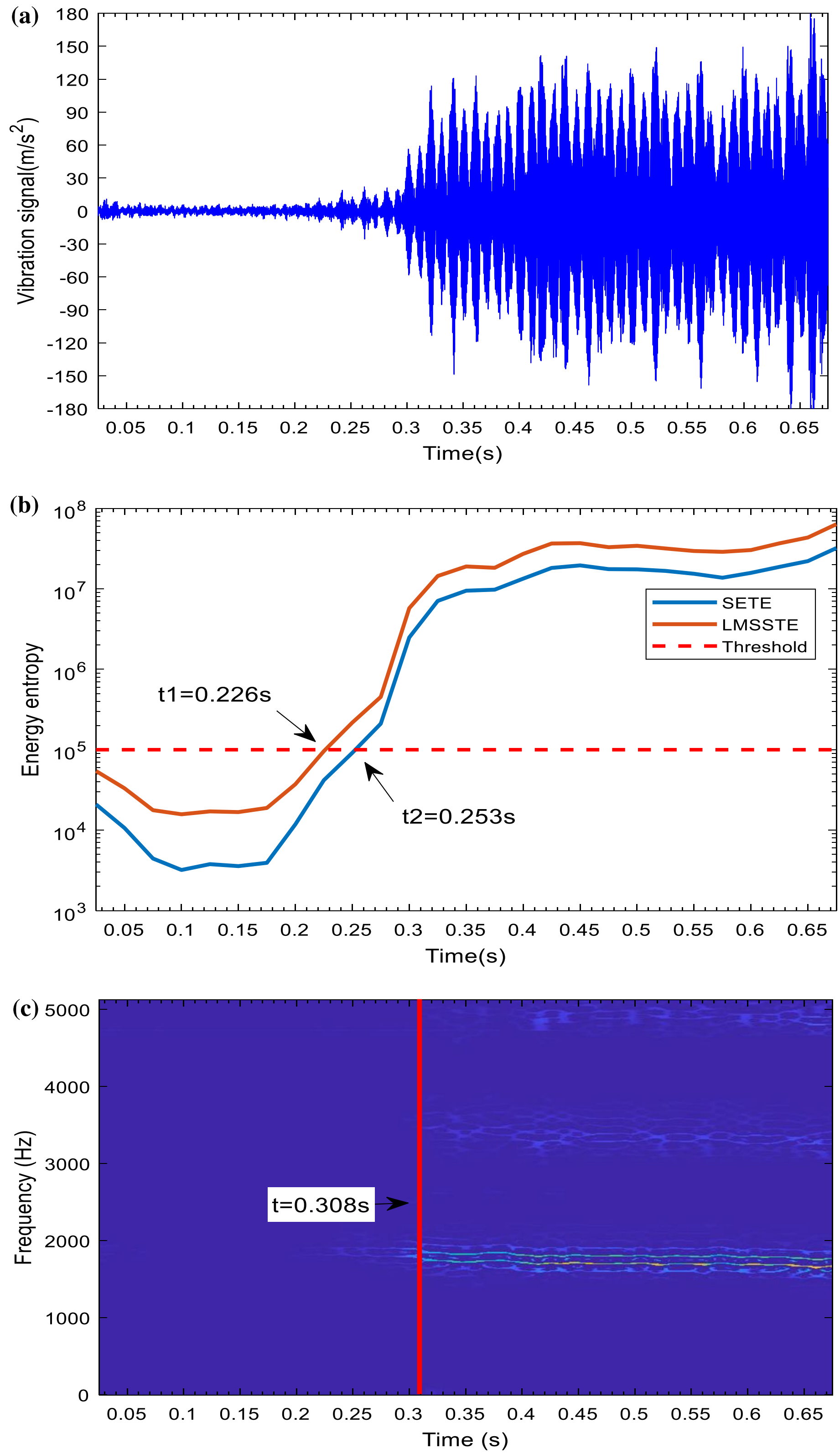

Fig. 6 The detection result and SET spectrogram for the vibration signals with spindle speed 3000 rpm and feed rate 6.0 mm/s

algorithm recognize the chatter 14 ms earlier than the synchroextracting-based method in reference Tao et al. (2019a).

Then, experimental results with different spindle speed and feed rate combinations were analyzed. The time-domain diagram, the identification result and the time–frequency spectrogram for the vibration signal with spindle speed 4500 rpm and feed rate 3.2 mm/s is presented in Fig. 4. The workpiece was aluminum alloy AL7075 as well. It can be seen from Fig. 4a that the amplitude of the vibration signal increases rapidly after $t = 0.281$ s, and the robotic drilling chatter occurs. With a short period time of chatter development, the amplitude of the vibration signal has exceeded 70 m/s^2. According to the identification result Fig. 4b, the proposed method recognizes the occurrence of chatter near $t1 = 0.242$ s. At the same time, the corresponding time–frequency spectrum Fig. 4c shows the obvious chatter frequency appears at $t = 0.293$ s. Consequently, it demonstrates that the vibration state of the robotic drilling system can be well recognized by the proposed chatter identification method. In addition, the result shows that the proposed identification algorithm detects the chatter 17 ms earlier than the synchroextracting-based method, which further verify the effectiveness of the proposed identification method.

Also, for the sake of further verifying the proposed LMSST-based chatter identification algorithm, robotic drilling tests with tool II and aluminum alloy 6061 under different drilling parameters were conducted. Figure 5 shows the time-domain diagram, the identification result and the time–frequency spectrogram for the vibration signal with spindle speed 3600 rpm and feed rate 3.6 mm/s. According to Fig. 5a, the amplitude of the vibration signal increases substantially after $t = 0.257$ s, and the chatter occurs during the robotic drilling process. As illustrated in Fig. 5b, the energy entropy is relatively small and grows slightly at the beginning stage. The energy entropy increases faster after $t = 0.101$ s, but then starts to decrease at $t = 0.152$ s. A closer look at Fig. 5a, b reveals that the energy entropy is very sensitive to changes in the amplitude of the vibration signal. Then, the energy entropy increases rapidly again after $t = 0.202$ s. Finally, the chatter is recognized at $t1 = 0.215$ s by the proposed identification algorithm, and $t2 = 0.239$ s by method in Tao et al. (2019a). The result demonstrates that the proposed identification algorithm detects the chatter earlier than the synchroextracting-based method. Meanwhile, the corresponding high-resolution time–frequency spectrum Fig. 5c shows the obvious chatter frequency appears near $t = 0.295$ s. Therefore, the proposed identification method can effectively recognize the chatter at its early transition stage, which is practical for the subsequent chatter suppression.

Figure 6 illustrates the time-domain diagram, the identification result and the high-resolution time–frequency spectrogram for the vibration signals with spindle speed 3000 rpm and feed rate 6.0 mm/s. The workpiece was also aluminum alloy AL6061. As shown in Fig. 6a, the amplitude of the vibration signal increases substantially after $t = 0.282$ s, and the chatter occurs during the robotic drilling process. After a short period time of rapid development, the amplitude of the vibration signal has exceeded 100 m/s^2. It is seen from Fig. 6b that the energy entropy decreases slowly in the beginning, and then remains essentially constant. After $t = 0.175$ s, it increases rapidly. According to Fig. 6b, the chatter is recognized near $t1 = 0.226$ s by the proposed identification algorithm. Meanwhile, the obvious chatter frequency appears at $t = 0.308$ s in the corresponding time–frequency spectrum Fig. 6c. Consequently, it demonstrates that the vibration state of the robotic drilling system can be well recognized by the proposed chatter identification method. In addition, it can be seen that the proposed identification algorithm detects the chatter 27 ms earlier than the synchroextracting-based method.

Conclusion

In this study, a novel method based on the matrix notch filter and local maximum synchrosqueezing transform has been proposed for the timely and accurate chatter identification of robotic drilling. The optimal matrix notch filter is designed to fully remove the spindle frequency and corresponding harmonic components from the measured vibration signal. The local maximum synchrosqueezing transform (LMSST) that achieves highly concentrated time–frequency representation and allows for perfect signal reconstruction is employed to obtain high-resolution time–frequency information of the non-stationary filtered acceleration signal. Then, the vibration signal is divided into finite equal-width frequency bands, and the corresponding sub-signal for each frequency band is obtained by summing the corresponding coefficient of the LMSST. Finally, the statistical energy entropy is calculated and utilized to accurately depict the non-uniformity of energy distribution during the chatter incubation process. Robotic drilling experiments with different drilling parameters and workpiece materials have been conducted to verify the effectiveness of the proposed method. The results demonstrate that the proposed method can effectively detect chatter at an early stage, and can detects chatter earlier than the synchroextracting-based method. In conclusion, the proposed robotic drilling chatter identification algorithm has a high potential for industrial applications.

Acknowledgements This work was partially supported by the National Key Research and Development Program of China (Grant Nos. 2017YFB1302601 and 2018YFB1306703).

References

Altintas, Y., Stepan, G., Merdol, D., & Dombovari, Z. (2008). Chatter stability of milling in frequency and discrete time domain. *CIRP Journal of Manufacturing Science and Technology, 1*(1), 35–44.

Aslan, D., & Altintas, Y. (2018). On-line chatter detection in milling using drive motor current commands extracted from CNC. *International Journal of Machine Tools and Manufacture, 132,* 64–80.

Bi, S., & Liang, J. (2011). Robotic drilling system for titanium structures. *International Journal of Advanced Manufacturing Technology, 54,* 767–774.

Bu, Y., Liao, W. H., Tian, W., Zhang, L., & Li, D. W. (2017). Modeling and experimental investigation of Cartesian compliance characterization for drilling robot. *International Journal of Advanced Manufacturing Technology, 91*(9–12), 3253–3264.

Cao, H., Yue, Y., Chen, X., & Zhang, X. (2017). Chatter detection in milling process based on synchro squeezing transform of sound signals. *International Journal of Advanced Manufacturing Technology, 89*(9–12), 2747–2755.

Chen, Y., & Dong, F. (2013). Robot machining: Recent development and future research issues. *International Journal of Advanced Manufacturing Technology, 66*(9–12), 1489–1497.

Cordes, M., Hintze, W., & Altintas, Y. (2019). Chatter stability in robotic milling. *Robotics and Computer-Integrated Manufacturing, 55,* 11–18.

Frommknecht, A., Kuehnle, J., Effenberger, I., & Pidan, S. (2017). Multi-sensor measurement system for robotic drilling. *Robotics and Computer-Integrated Manufacturing, 47,* 4–10.

Fu, Y., Zhang, Y., Gao, H., Mao, T., Zhou, H., Sun, R., et al. (2019). Automatic feature constructing from vibration signals for machining state monitoring. *Journal of Intelligent Manufacturing, 30*(3), 995–1008.

Fu, Y., Zhang, Y., Zhou, H., Li, D., Liu, H., Qiao, H., et al. (2016). Timely online chatter detection in end milling process. *Mechanical Systems and Signal Processing, 75,* 668–688.

Han, D., & Zhang, X. H. (2010). Optimal matrix filter design with application to filtering short data records. *IEEE Signal Processing Letters, 17*(5), 521–524.

Huang, P., Li, J., Sun, J., & Zhou, J. (2013). Vibration analysis in milling titanium alloy based on signal processing of cutting force. *International Journal of Advanced Manufacturing Technology, 64*(5–8), 613–621.

Iglesias, I., Sebastián, M. A., & Ares, J. E. (2015). Overview of the state of robotic machining: Current situation and future potential. *Procedia Engineering, 132,* 911–917.

Insperger, T., & Stepan, G. (2004). Updated semi-discretization method for periodic delay-differential equations with discrete delay. *International Journal for Numerical Methods in Biomedical Engineering, 61*(1), 117–141.

Ji, Y., Wang, X., Liu, Z., Wang, H., Jiao, L., Wang, D., et al. (2018). Early milling chatter identification by improved empirical mode decomposition and multi-indicator synthetic evaluation. *Journal of Sound and Vibration, 433,* 138–159.

Ji, Y., Wang, X., Liu, Z., Yan, Z., Jiao, L., Wang, D., et al. (2017). EEMD-based online milling chatter detection by fractal dimension and power spectral entropy. *International Journal of Advanced Manufacturing Technology, 92*(1–4), 1185–1200.

Kuljanic, E., Totis, G., & Sortino, M. (2009). Development of an intelligent multisensor chatter detection system in milling. *Mechanical Systems and Signal Processing, 23*(5), 1704–1718.

Lamraoui, M., Thomas, M., & El Badaoui, M. (2014a). Cyclostationarity approach for monitoring chatter and tool wear in high speed milling. *Mechanical Systems and Signal Processing, 44*(1–2), 177–198.

Lamraoui, M., Thomas, M., El Badaoui, M., & Girardin, F. (2014b). Indicators for monitoring chatter in milling based on instantaneous angular speeds. *Mechanical Systems and Signal Processing, 44*(1–2), 72–85.

Li, Z. Q., & Liu, Q. (2008). Solution and analysis of chatter stability for end milling in the time-domain. *Chinese Journal of Aeronautics, 21,* 169–178.

Lin, Y., Zhao, H., & Ding, H. (2017). Posture optimization methodology of 6R industrial robots for machining using performance evaluation indexes. *Robotics and Computer-Integrated Manufacturing, 48,* 59–72.

Liu, H., Chen, Q., Li, B., Mao, X., Mao, K., & Peng, F. (2011). On-line chatter detection using servo motor current signal in turning. *Science China Technological Sciences, 54*(12), 3119–3129.

Liu, Y., Wang, X., Lin, J., & Zhao, W. (2016). Early chatter detection in gear grinding process using servo feed motor current. *International Journal of Advanced Manufacturing Technology, 83*(9–12), 1801–1810.

Liu, C., Zhu, L., & Ni, C. (2017). The chatter identification in end milling based on combining EMD and WPD. *International Journal of Advanced Manufacturing Technology, 91*(9–12), 3339–3348.

Liu, C., Zhu, L., & Ni, C. (2018). Chatter detection in milling process based on VMD and energy entropy. *Mechanical Systems and Signal Processing, 105,* 169–182.

Lu, K., Jing, M., Zhang, X., Dong, G., & Liu, H. (2015). An effective optimization algorithm for multipass turning of flexible workpieces. *Journal of Intelligent Manufacturing, 26,* 831–840.

Mei, B., Zhu, W., Yuan, K., & Ke, Y. (2015). Robot base frame calibration with a 2D vision system for mobile robotic drilling. *International Journal of Advanced Manufacturing Technology, 80*(9–12), 1903–1917.

Mousavi, S., Gagnol, V., Bouzgarrou, B. C., & Ray, P. (2017). Dynamic modeling and stability prediction in robotic machining. *International Journal of Advanced Manufacturing Technology, 88*(9–12), 3053–3065.

Munoa, J., Beudaert, X., Dombovari, Z., Altintas, Y., Budak, E., Brecher, C., et al. (2016). Chatter suppression techniques in metal cutting. *CIRP Annals—Manufacturing Technology, 65*(2), 785–808.

Piskorowski, J. (2010). Digital q-varying notch IIR filter with transient suppression. *IEEE Transactions on Instrumentation and Measurement, 59*(4), 866–872.

Piskorowski, J. (2012). Suppressing harmonic powerline interference using multiple-notch filtering methods with improved transient behavior. *Measurement, 45*(6), 1350–1361.

Pour, M., & Torabizadeh, M. A. (2016). Improved prediction of stability lobes in milling process using time series analysis. *Journal of Intelligent Manufacturing, 27*(3), 665–677.

Qin, C. J., Tao, J. F., Li, L., & Liu, C. L. (2017a). An Adams-Moulton-based method for stability prediction of milling processes. *International Journal of Advanced Manufacturing Technology, 89*(9–12), 3049–3058.

Qin, C. J., Tao, J. F., & Liu, C. L. (2017b). Stability analysis for milling operations using an Adams-Simpson-based method. *International Journal of Advanced Manufacturing Technology, 92*(1–4), 969–979.

Qin, C. J., Tao, J. F., & Liu, C. L. (2018). A predictor-corrector-based holistic-discretization method for accurate and efficient milling stability analysis. *International Journal of Advanced Manufacturing Technology, 96*(5–8), 2043–2054.

Qin, C. J., Tao, J. F., & Liu, C. L. (2019). A novel stability prediction method for milling operations using the holistic-interpolation scheme. *Proceedings—IMechE Part C, Journal of Mechanical Engineering Science, 233*(13), 4463–4475.

Somkiat, T. (2011). Advanced in detection system to improve the stability and capability of CNC turning process. *Journal of Intelligent Manufacturing, 22,* 843–852.

Sun, Y. X., & Xiong, Z. H. (2016). An optimal weighted wavelet packet entropy method with application to real-time chatter detection. *IEEE-ASME Transactions on Mechatronics, 21*(4), 2004–2014.

Tangjitsitcharoen, S., Saksri, T., & Ratanakuakangwan, S. (2015). Advance in chatter detection in ball end milling process by utilizing wavelet transform. *Journal of Intelligent Manufacturing, 26*(3), 485–499.

Tao, J. F., Qin, C. J., & Liu, C. L. (2019a). A synchroextracting-based method for early chatter identification of robotic drilling process. *International Journal of Advanced Manufacturing Technology, 100*(1–4), 273–285.

Tao, J., Qin, C., Xiao, D., Shi, H., & Liu, C. (2019b). A pre-generated matrix-based method for real-time robotic drilling chatter monitoring. *Chinese Journal of Aeronautics*. https://doi.org/10.1016/j.cja.2019.09.001.

Thaler, T., Potočnik, P., Bric, I., & Govekar, E. (2014). Chatter detection in band sawing based on discriminant analysis of sound features. *Applied Acoustics, 77,* 114–121.

Tong, X., Liu, Q., Pi, S., & Xiao, Y. (2019). Real-time machining data application and service based on IMT digital twin. *Journal of Intelligent Manufacturing*. https://doi.org/10.1007/s10845-019-01500-0.

Tseng, C. C., & Pei, S. C. (2001). Stable IIR notch filter design with optimal pole placement. *IEEE Transactions on Signal Processing, 49*(11), 2673–2681.

Vaccaro, R. J., & Harrison, B. F. (1996). Optimal matrix-filter design. *IEEE Transactions on Signal Processing, 44*(3), 705–709.

Wan, S., Li, X., Chen, W., & Hong, J. (2018). Investigation on milling chatter identification at early stage with variance ratio and Hilbert-Huang transform. *International Journal of Advanced Manufacturing Technology, 95,* 3563–3573.

Wang, G., Dong, H., Guo, Y., & Ke, Y. (2017). Chatter mechanism and stability analysis of robotic boring. *International Journal of Advanced Manufacturing Technology, 91,* 411–421.

Wang, G., Dong, H., Guo, Y., & Ke, Y. (2018). Early chatter identification of robotic boring process using measured force of dynamometer. *International Journal of Advanced Manufacturing Technology, 94*(1–4), 1243–1252.

Yang, K., Wang, G., Dong, Y., Zhang, Q., & Sang, L. (2019). Early chatter identification based on an optimized variational mode decomposition. *Mechanical Systems and Signal Processing, 115,* 238–254.

Ye, J., Feng, P., Xu, C., Ma, Y., & Huang, S. (2018). A novel approach for chatter online monitoring using coefficient of variation in machining process. *International Journal of Advanced Manufacturing Technology, 96*(1–4), 287–297.

Yu, G., Wang, Z. H., Zhao, P., & Li, Z. (2019). Local maximum synchrosqueezing transform: An energy-concentrated time-frequency analysis tool. *Mechanical Systems and Signal Processing, 117,* 537–552.

Yu, G., Yu, M., & Xu, C. (2017). Synchroextracting transform. *IEEE Transactions on Industrial Electronics, 64*(10), 8042–8054.

Yuan, L., Pan, Z., Ding, D., Sun, S., & Li, W. (2018). A review on chatter in robotic machining process regarding both regenerative and mode coupling mechanism. *IEEE-ASME Transactions on Mechatronics, 23*(5), 2240–2251.

Yuan, L., Sun, S., Pan, Z., Ding, D., Gienke, O., & Li, W. (2019). Mode coupling chatter suppression for robotic machining using semi-active magnetorheological elastomers absorber. *Mechanical Systems and Signal Processing, 117,* 221–237.

Zeng, Y., Tian, W., Li, D., He, X., & Liao, W. (2017). An error-similarity-based robot positional accuracy improvement method for a robotic drilling and riveting system. *International Journal of Advanced Manufacturing Technology, 88*(9–12), 2745–2755.

Zhang, Z., Li, H., Meng, G., Tu, X., & Cheng, C. (2016). Chatter detection in milling process based on the energy entropy of VMD and WPD. *International Journal of Machine Tools and Manufacture, 108,* 106–112.